Supporting Information

Deposition Kinetics of Colloidal Manganese Dioxide onto Representative Surfaces in Aquatic Environments: The Role of Humic Acid and Biomacromolecules

Xiaoliu Huangfu[†*], Chengxue Ma[†], Ruixing Huang[†], Qiang He[†*], Caihong Liu[†], Jian Zhou[†], Jin Jiang[‡], Jun Ma[‡], Yinying Zhu[†], Muhua Huang[†]

[†] *Key Laboratory of Eco-environments in the Three Gorges Reservoir Region, Ministry of Education, Faculty of Urban Construction and Environmental Engineering, National Centre for International Research of Low-Carbon and Green Buildings, Chongqing University, Chongqing 400044, China*

[‡] *State Key Laboratory of Urban Water Resource and Environment, School of Municipal and Environmental Engineering, Harbin Institute of Technology, Harbin 150090, China*

Corresponding Authors: Dr. Xiaoliu Huangfu and Professor Qiang He

Phone: 86-23-65120980; fax: 86-23-65120980; e-mail: hfxl@cqu.edu.cn (X. H.); hq0980@126.com (Q. H.)

Summary

Eighteen pages, including 15 figures, 5 tables, and 4 texts.

Text S1. Cleaning Methods for QCM-D Crystal Sensors:

1. QSX 303 Silicon Dioxide , and QSX 309 Aluminum Oxide

a. UV/ozone treatment for 20 minutes.

b. Immerse the sensor surface in the solution of 2% SDS for 30 min in room temperature.

c. Rinse with DDI water and dry with nitrogen gas.

d. UV/ozone treatment for 20 minutes.

Note that for crystal sensors used in coated surfaces deposition experiments, the crystal sensors were immersed in 1% Hellmanex II instead of 2% SDS solution.

2. QSX 326 Iron Oxide

a. Sonicate the sonsor surface in methanol for 15 minutes.

b. Rinse with DDI water.

c. Dry with nitrogen gas.

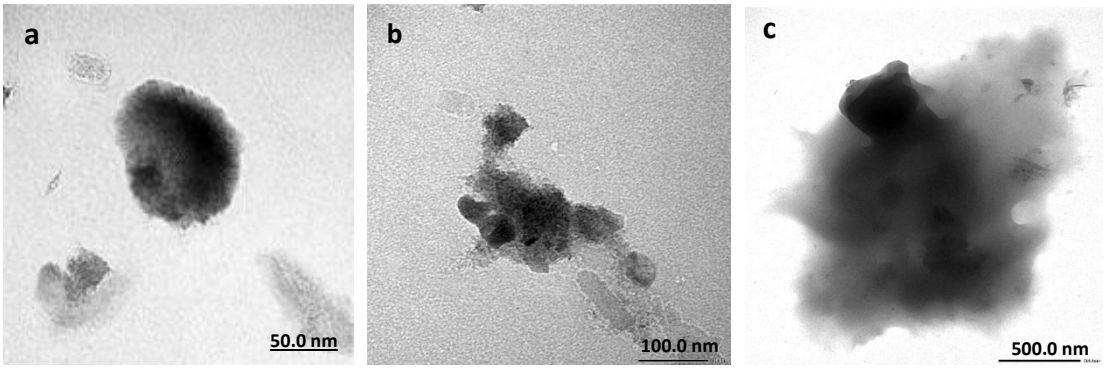

Figure S1 Representative TEM micrograph of MnO_2 aggregates

Text S2 Deposition kinetics of colloidal MnO_2 on PLL coating environmental surfaces

To achieve fast deposition of MnO_2 colloids on tested surfaces, PLL was selected to coat on all three tested surfaces. PLL was dissolved in the desired electrolyte solutions at the concentration of 0.1g/L. The crystal was coated by PLL by flowing 2 mL of the electrolyte solution containing PLL across the substrate surface. The solution was injected into the system for at least 20 min at 0.15 mL/min. During PLL deposition, $\Delta f_{(3)}$ first decreased and then plateaued, indicating that the surface was completely covered with PLL. Then, the PLL-coated surface was equilibrated with 2 mL of the background electrolyte before the deposition of MnO_2 colloidal suspensions onto the PLL-coated surface.

The representative deposition profiles ould be found in Figure S2, S3, and S4, and the corresponding r_f were presented in Figure S5. Generally, in Figure S2, S3, and S4, similar frequency shifts were observed when MnO_2 colloids deposition on selected surfaces at $NaNO_3$ concentration of 1 mM, 7 mM, 15 mM, and 17 mM, respectively. Our previous work had indicated that aggregation of colloidal MnO_2 was ignorable when $NaNO_3$ concentration lower than 10 mM, whereas obvious aggregation could be observed when $NaNO_3$ concentration was higher than 15 mM.[1] Deposition results here were in agreement with this observation. For all favorable deposition, the frequency shifts obtained from QCM-D were similar at 1 mM and 7 mM $NaNO_3$, which decreased lightly in the presence of 15 mM $NaNO_3$ and decreased notably when $NaNO_3$ concentration was higher than 15 mM, i.e., 17 mM. Data in Figure S5 revealed that r_f values decreased dramatically after a plateau when $NaNO_3$ concentration was higher than 10 mM for all three PLL coating surfaces. The increase in salt concentration leading to a decrease in the magnitude of attractive electrostatic interactions between oppositely charged colloids and PLL surface might be mainly responsible for this decrease in the deposition under corresponding condition. MnO_2 colloidal aggregation resulting in lower diffusivities at further high Na^+ concentrations discussed before can also lead to this hindered deposition.

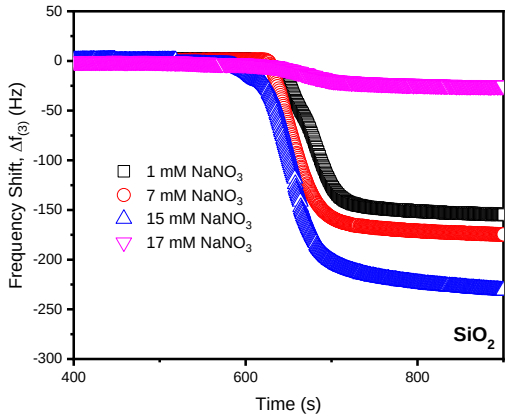

Figure S2. Representative frequency shift ($\Delta f_{(3)}$) obtained by QCM-D as a function of $NaNO_3$ concentration at pH 6.0 when colloidal MnO_2 was deposited on PLL coated SiO_2 surface.

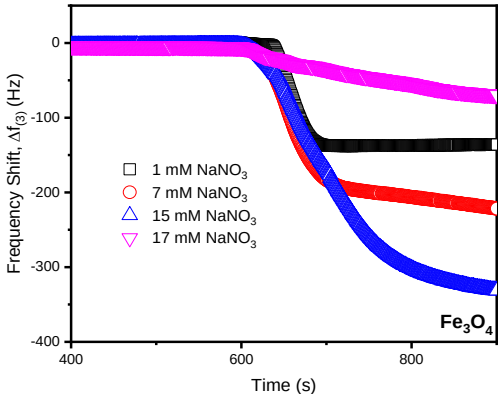

Figure S3. Representative frequency shift ($\Delta f_{(3)}$) obtained by QCM-D as a function of $NaNO_3$ concentration at pH 6.0 when colloidal MnO_2 was deposited on PLL coated Fe_3O_4 surface.

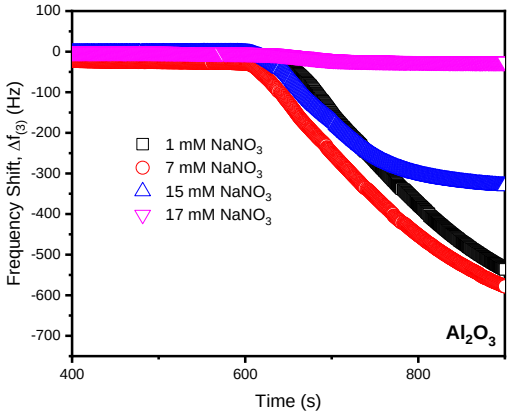

Figure S4. Representative frequency shift (Δf_3) obtained by QCM-D as a function of $NaNO_3$ concentration at pH 6.0 when colloidal MnO_2 was deposited on PLL coated Al_2O_3 surface.

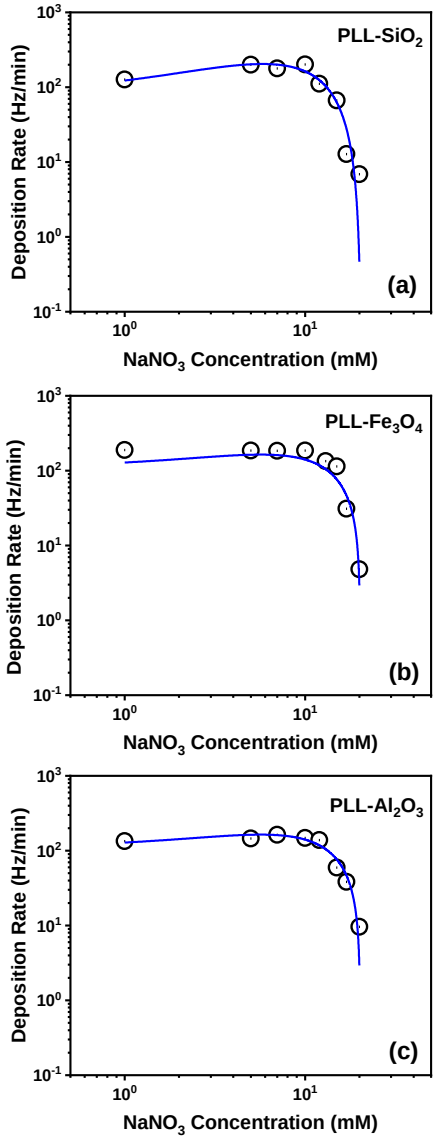

Figure S5. Favorable deposition rates of colloidal MnO_2 onto PLL-coated surfaces (i.e., SiO_2 surface, Fe_3O_4 surface, and Al_2O_3surface) as function of $NaNO_3$ concentration at pH 6.0.

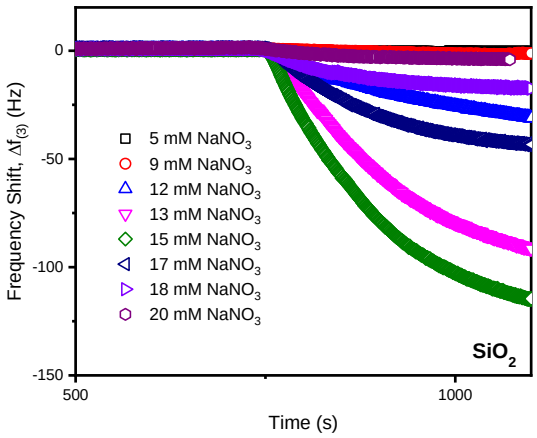

Figure S6. Representative frequency shift ($\Delta f_{(3)}$) obtained by QCM-D as a function of $NaNO_3$ concentration at pH 6.0 when colloidal MnO_2 was deposited on bare SiO_2 surface.

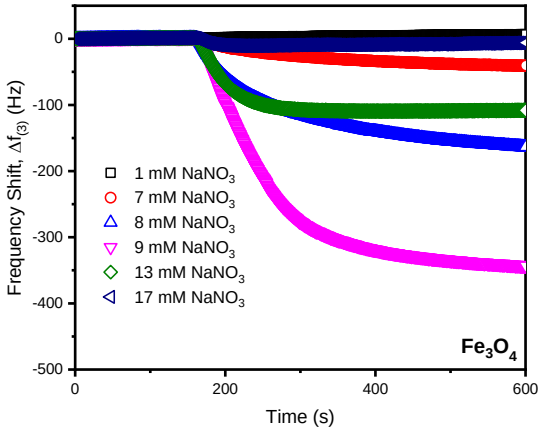

Figure S7. Representative frequency shift ($\Delta f_{(3)}$) obtained by QCM-D as a function of $NaNO_3$ concentration at pH 6.0 when colloidal MnO_2 was deposited on bare Fe_3O_4 surface.

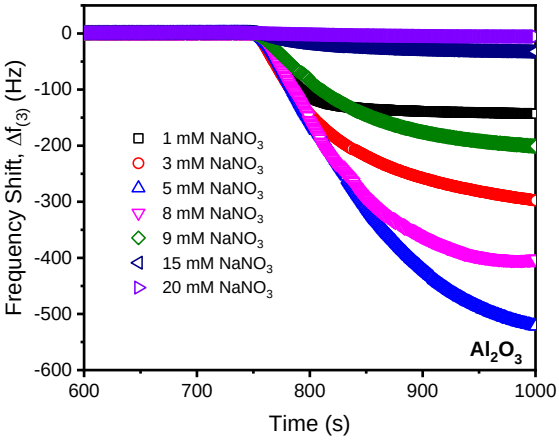

Figure S8. Representative frequency shift ($\Delta f_{(3)}$) obtained by QCM-D as a function of $NaNO_3$ concentration at pH 6.0 when colloidal MnO_2 was deposited on bare Al_2O_3 surface.

Text S3 Aggregation experiments of colloidal MnO_2

For aggregation experiments of MnO_2 colloids in the absence and presence of macromolecules, time-resolved dynamic light scattering (TR-DLS) (Nano ZS90, Malvern, UK) operating with a He-Ne laser at a wavelength of 633 nm and a detection angle of 90° was used to investigate the early stage increase of colloidal averaged hydrodynamic diameter (Dh) at various $NaNO_3$ concentrations. The MnO_2 solution was diluted to 1mM and the concentration of HA, alginate and BSA was controlled at 5 mg/L of TOC. Detailed protocals of aggregation measurement and determination of aggregation kinetics can be found in our previous publication.[1]

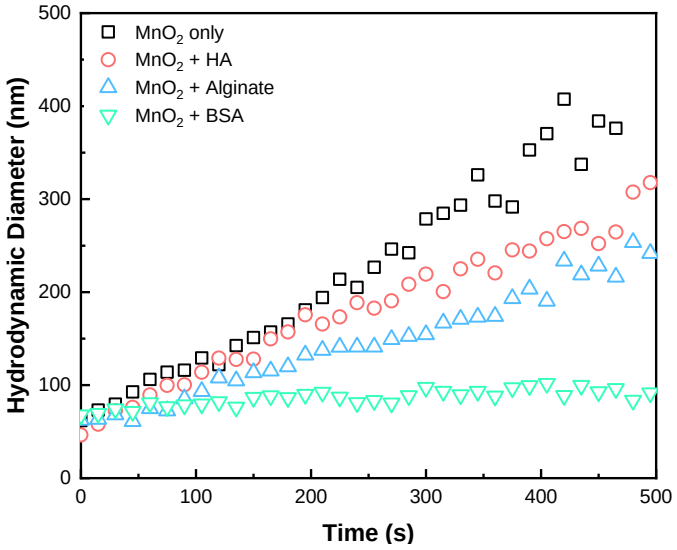

Figure S9. Representaitive aggregation profiles of MnO_2 colloids in 15 mM $NaNO_3$. Aggregation experiments were conducted at pH 6.0 and 25 °C.

Table S1 . The initial aggregation rate of MnO_2 colloids in the presence of HA, Alginate and BSA as a function of $NaNO_3$.

Na concentration	**Aggregation Rate (nms^{-1})**			
(mM)	MnO_2 only	MnO_2 +HA	MnO_2+Alginate	MnO_2+BSA
5	0.02±0.01	-	-	-
10	0.05±0.01	0.05±0.01	0.04±0.01	-
15	0.73±0.05	0.49±0.11	0.34±0.07	0.06±0.02
17	1.30±0.12	1.09±0.16	1.19±0.10	0.24±0.11
20	3.01±0.31	2.71±0.24	2.38±0.25	0.41±0.16
30	5.74±0.49	3.42±0.41	3.38±0.32	2.10±0.26
50	5.28±0.63	3.81±0.46	3.96±0.41	1.85±0.19

Table S2. Zeta potential (mV) of MnO_2 colloids and SiO_2, Al_2O_3, and Fe_3O_4 over a range of ionic strength.

	$NaNO_3$ concentraion (mM)					**References**
	1	5	10	15	20	
MnO_2 colloids	-58.72	-48.4	-35.5	-33.2	-30.9	Huangfu, X. L. etc [1]
SiO_2	-80	-66.8	-50.4	-49.1	-47.2	Thomas W. Healy [2]
Al_2O_3	40.6	45.4	51.4	52.06	52.73	Reyes Bahena, J. L.[3]
Fe_3O_4	-17.7	-15	-11.7	-8.4	-5	Murat Erdemoğlu [4]

Text S4. Calculation of DLVO and EDLVO Interaction Energy for MnO_2 colloids approaching Surfaces in the Absence of Macromolecules

1. DLVO Theory

To further interprete deposition kinetics of colloidal MnO_2 on selected environmental surfaces, classical DLVO was employed for calculating the interaction energy when they approched to these three surfaces. The main interactions acting on a NP include van der Waals energy (V_{VDW}), the electrstatic energy (i.e., electric double layer energy, V_{EDL}). The total interaction energy (V_T) and modified interaction energy ($V_{T\text{-}modified}$) could be calculated using the following equations:[5]

$$V_T = V_{VDW} + V_{EDL} \quad \text{(S1)}$$

where V_{VDW} is the van der Waals attractive energy between a particle and a surface:

$$V_{VDW}(h) = -\frac{A_{123} a_p}{6h(1+14h/\lambda)} \quad \text{(S2)}$$

where A_{123} is Hamarker constant for the deposition of a nanoparticle of composition "1" onto a surface of composition "3" when suspended in a medium "2"; a_p is particle radius. h surface-to-surface separation distance; λ is characteristic wavelength, 100 nm. V_{EDL} could be calculated by:

$$V_{EDL}(h) = 64\pi\varepsilon_0\varepsilon_r a_p (k_B T/ze)^2 \Gamma_1 \Gamma_2 \exp(-\kappa h) \quad \text{(S3)}$$

where ε_0 is dielectric permittivity in vacuum, 8.85×10^{-12} F/m; ε_r is relative dielectric permittivity of solution 78.5; k_B Boltzmann constant, 1.3805×10^{-23} J/K; T is absolute temperature, T=298.15 K; $_z$ counterion valence, z=1; e is electron charge, 1.602×10^{-19} C; Γ_1, Γ_2 is dimensionless surface potential for particle or collector presented in Table S2; κ is inverse Debye length.

$$\Gamma_i = \tanh\left({ze\psi_i}/{4k_BT}\right) \quad \text{(S4)}$$

where ψ_i is surface potential.

$$\kappa = \left(\frac{2e^2N_AI}{\varepsilon_0\varepsilon_r k_BT}\right)^{1/2} \quad \text{(S5)}$$

where N_A Avogadro constant,6.022×10^{23}; I is ionic strength.

2. Extended DLVO Interaction-Energy Calculations

In order to better understand the distinct impacts of humic acid and biomacromolecules on the deposition behavior of the $nMnO_2$ on environmental surfaces at various conditions, the DLVO interaction energy calculations were modified by the incorporation of a steric repulsive energy based on the Flory-Krigbaum theory when MnO_2 colloids approached to selected surfaces in the presence of three organic matters. The total steric interaction energy between a polymer coated colloid and an uncoated collector surface includes two components: a repulsive osmotic energy term, V_{osm} and an elastic repulsive energy, V_{elas}. V_{osm} is due to the exclusion of water molecules surrounding the polymers on the close colloid-surface approach (or compression of a macromolecular layer on a particle contacting a nonadsorbing surface). V_{elas} arises as the adsorbed macromolecule layers below the thickness of the unperturbed layer (l) polymer chains are compressed and leads to the elastic repulsion. The expressions for

V_{osm} and V_{elas} was given by Vincent[6] the interaction energy between two identical particles with coating of uniform segment density, as:[7]

$$\frac{V_{osm}}{k_BT} = \frac{4\pi a_p}{v_1}\phi_p^2\left(\frac{1}{2}-\chi\right)l^2\left(\frac{h}{2l}-\frac{1}{4}-ln\left(\frac{h}{l}\right)\right) \qquad h<l \qquad \text{(S6)}$$

$$\frac{V_{elas}}{k_BT} = \frac{2\pi a_p}{M_W}\phi_p l^2\rho_p\left[\frac{h}{l}ln\left(\frac{h}{d}\left(\frac{3-\frac{h}{l}}{2}\right)^2\right)-6\,ln\left(\frac{3-\frac{h}{l}}{2}\right)+3\left(1-\frac{h}{l}\right)^2\right] \; h<l \qquad \text{(S7)}$$

Where $v_1$is the volume of a solvent molecule (0.03 nm^3). [8] χ is the Flory-Huggins solvency parameter, which was assumed to be 0.45, 0.465 and 0.49 for HA, alginate and BSA respectively;[9,10] l is the thickness of NOM covered on the $nMnO_2$ surface and was estimated to be 30.2 nm, 24.3 nm and 38.9 nm for HA, alginate and BSA respectively by fitting the Ohshima's soft particle model, which can be found in our previous publication;[11] h is colloids-to-surface separation distance; M_W is the molecular weight of the macromolecules[12], and ρ_p is the polymer density. ϕ_p is the calculated volume fraction of polymer within the brush layer.

$$\phi_p = 3\frac{\Gamma_{max}{a_p}^2}{\rho_p\left[\left(l+a_p\right)^3-{a_p}^3\right]} \qquad \text{(S8)}$$

Γ_{max} is the maximum surface concentration (Kg/m^2). The theoretical specific surface area of $nMnO_2$ 144 m^2/g was used here. Based on the $nMnO_2$ surface area and the adsorption data of to the $nMnO_2$ presented in prevous study.[11] After calculation, the Γ_{max} for HA, alginate and BSA was 6.84×10^{-7} Kg/m^2, 6.68×10^{-7} Kg/m^2 and 1.67×10^{-6} Kg/m^2, respectively. The volume density for HA, alginate and BSA was estimated to be 8.74×10^{-3}, 8.48×10^{-3} and 1.06×10^{-2}, respectively.

The total modified interaction energy ($V_{T\text{-}Extended}$) could be calculated using the following equations:

$$V_{T\text{-}Extended} = V_{VDW} + V_{EDL} + V_{osm} + V_{elas} \qquad \text{(S9)}$$

3. Calculation of Hamaker Constants

Hamaker constants for colloidal MnO_2 is calculated by[13]:

$$A_{123} = (\sqrt{A_{33}} - \sqrt{A_{22}})(\sqrt{A_{11}} - \sqrt{A_{22}}) \quad \text{(S10)}$$

Where A_{11}, A_{22}, and A_{33} is the Hamaker constants of "1", "2", and "3" in vacuum, respectively required for use in these equations. Additionally, A_{121} is the Hamaker constant for the aggregation of two nanoparticles of composition "1" when suspended in a medium "2". A_{121} can be calculated by[13]:

$$A_{121} = (\sqrt{A_{22}} - \sqrt{A_{11}})^2 \quad \text{(S11)}$$

Table S3. Hamaker constant used for DLVO energy calculation

NO.	Hamaker constant	System	Value ($\times 10^{-20}$, J)	References
1	A_{121}	$nMnO_2$-water-$nMnO_2$	7.84	Huangfu, X. L. etc [11]
2	A_{22}	water	3.70	Israelachvili, J. N. [14]
	A_{33}	quartz	8.86	Bergström, L. [15]
4	A_{33}	Al_2O_3	14.50 (IKK), 15.20 (SNP)	Bergström, L. [15]
5	A_{121}	Fe_3O_4-water-Fe_3O_4	3.3	Faure B. etc [16]
6	A_{33}	Fe_3O_4	4.3	Faure B. etc [16] Faure B. etc [16]
7	A_{123}	$nMnO_2$-water-SiO_2	2.94	This study
8	A_{123}	$nMnO_2$-water- Al_2O_3	5.27	This study
9	A_{123}	$nMnO_2$-water- Fe_3O_4	5.09	This study

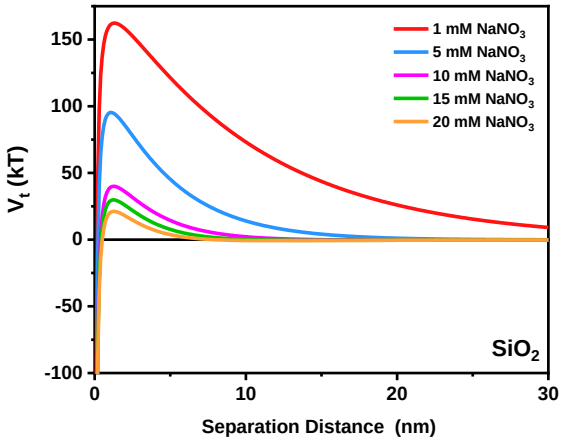

Figure S10. DLVO interaction energy profiles for MnO_2 colloids approaching silica surface as function of 1 mM, 5 mM, 10 mM, 15 mM, and 20 mM $NaNO_3$ at pH 6.0.

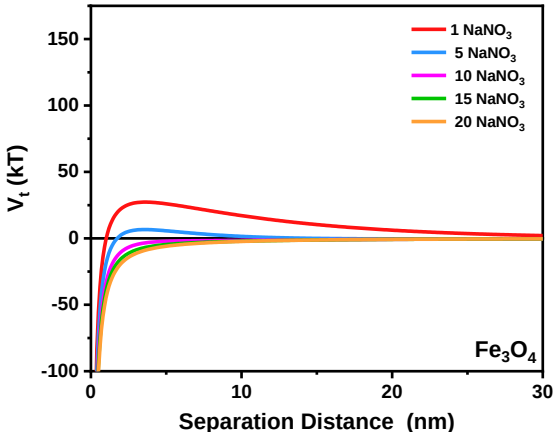

Figure S11. DLVO interaction energy profiles for MnO_2 colloids approaching magnetite surface as function of 1 mM, 5 mM, 10 mM, 15 mM, and 20 mM $NaNO_3$ at pH 6.0.

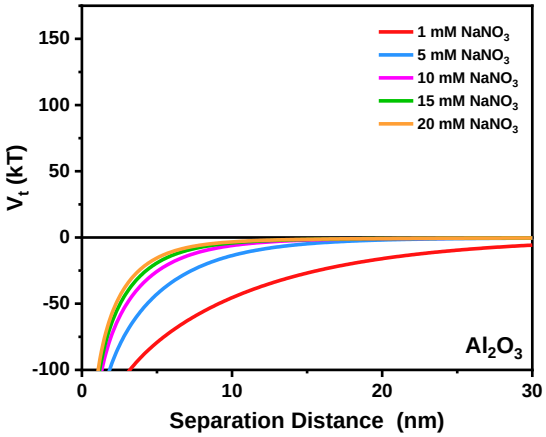

Figure S12. DLVO interaction energy profiles for MnO_2 colloids approaching alumina surface as function of 1 mM, 5 mM, 10 mM, 15 mM, and 20 mM $NaNO_3$ at pH 6.0.

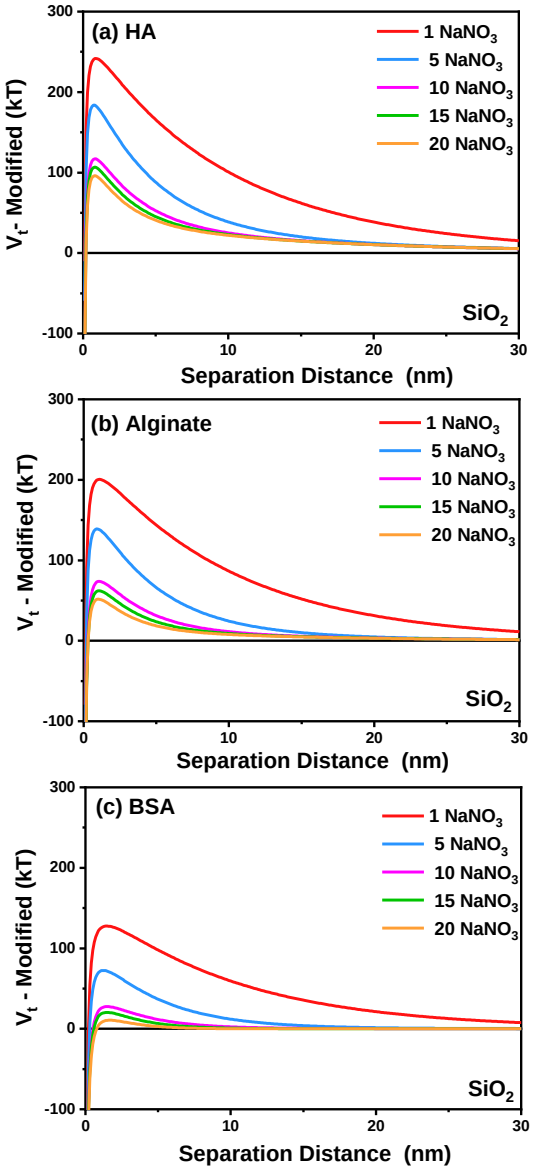

Figure S13. Extended DLVO interaction energy profiles for MnO_2 colloids approaching silica surface in the presence of (a) HA, (b) alginate and (c) BSA as function of 1 mM, 5 mM, 10 mM, 15 mM, and 20 mM $NaNO_3$ at pH 6.0.

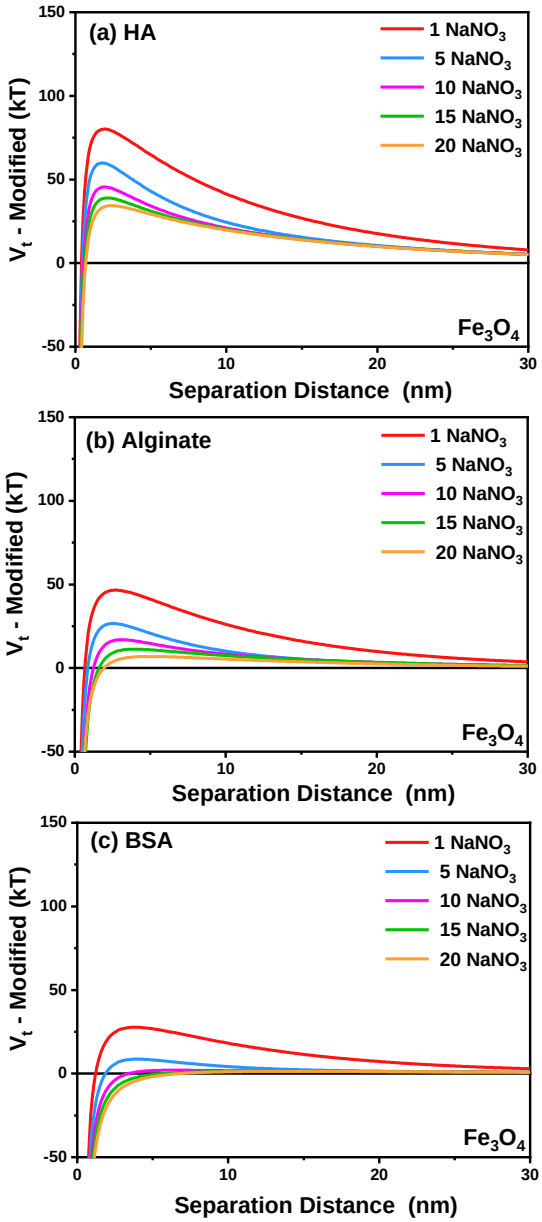

Figure S14. Extended DLVO interaction energy profiles for MnO_2 colloids approaching magnetite surface in the presence of (a) HA, (b) alginate and (c) BSA as function of 1 mM, 5 mM, 10 mM, 15 mM, and 20 mM $NaNO_3$ at pH 6.0.

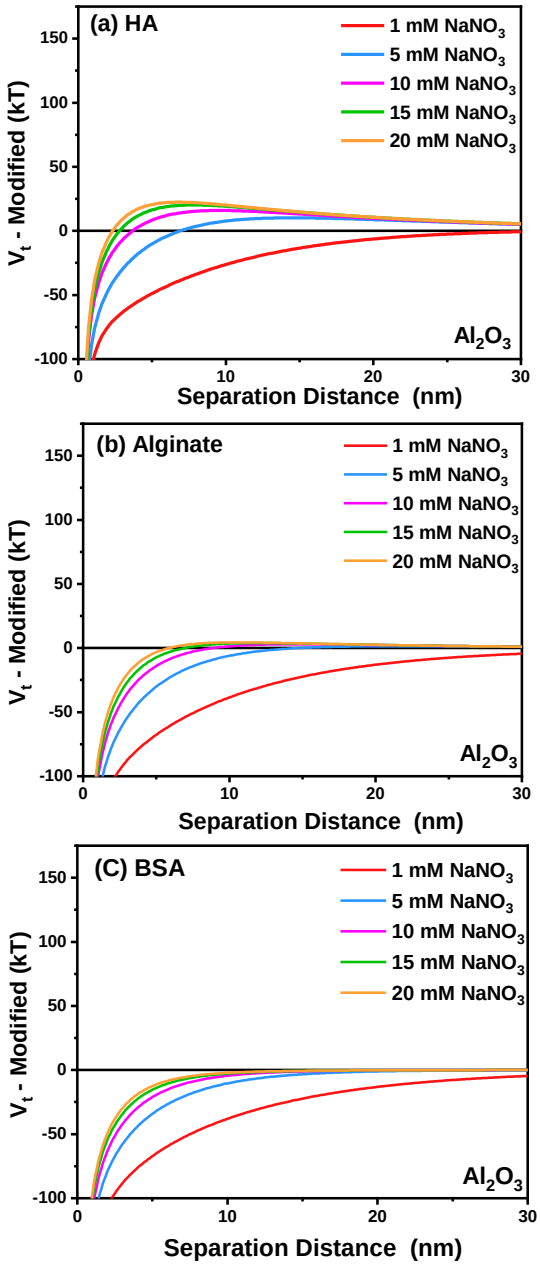

Figure S15. Extended DLVO interaction energy profiles for MnO_2 colloids approaching alumina surface in the presence of (a) HA, (b) alginate and (c) BSA as function of 1 mM, 5 mM, 10 mM, 15 mM, and 20 mM $NaNO_3$ at pH 6.0.

Table S4. Deposition rate of BSA, MnO_2 colloids, and MnO_2 colloids+BSA onto silica, magnetite and alumina surface, i.e., $|r_{f,BSA}|$, $|r_{f,MnO2\ colloids}|$ and $|r_{f,MnO2\ colloids+BSA}|$, respectively.

Surface Type	Na concentration (mM)	Deposition Rate (Hz/min)			
		$\|r_{f,BSA}\|$	$\|r_{f,MnO_2}\|$	$\|r_{f,MnO_2+BSA}\|$	$\|r_{f,BSA}\|+\|r_{f,MnO_2}\|$
SiO_2	5	4.302	0.528	2.442	4.830
	10	4.122	4.704	48.177	8.826
	15	3.324	42.756	116.094	46.08
	20	1.02	0.834	39.213	1.854
	50	0.564	-	3.126	-
Fe_3O_4	5	2.268	14.388	28.986	16.656
	10	1.488	185.112	172.122	186.6
	15	1.32	101.736	208.65	103.056
	20	1.134	3.444	181.23	4.578
	50	0.99	-	4.65	-
Al_2O_3	5	4.302	200.706	172.122	205.008
	10	3.517	109.982	208.65	113.994
	15	1.338	31.236	194.55	32.574
	20	1.068	1.594	117.924	2.662
	50	0.684	-	2.358	-

$|r_{f,BSA}|$ refers to the deposition rate of BSA macromolecule onto three surfaces.

$|r_{f,MnO_2\ colloids}|$ refers to the deposition rate of MnO_2 colloids onto three surfaces without background macromolecules.

$|r_{f,\ MnO_2+BSA}|$ refers to the deposition rate of MnO_2 colloids in the presence of BSA.

$|r_{f,BSA}|+|r_{f,MnO_2}|$ refers to the the sum of $|r_{f,BSA}|$ and $|r_{f,\ MnO_2\ colloids}|$.

Table S5. EPM of MnO_2 colloids in the presence of HA, Alginate and BSA as a function of $NaNO_3$.

Na concentration (mM)	EPM($10^{-8}m^{-2}V^{-1}s^{-1}$)			
	MnO_2 only	MnO_2 +HA	MnO_2+Alginate	MnO_2+BSA
5	-3.26±0.36	-3.48±0.37	-3.07±0.31	-2.14±0.19
10	-2.68±0.33	-2.83±0.35	-2.59±0.28	-2.08±0.23
15	-2.46±0.31	-2.71±0.29	-2.50±0.27	-2.01±0.39
20	-2.31±0.25	-2.68±0.31	-2.42±0.24	-1.96±0.19
30	-2.19±0.22	-2.57±0.28	-2.29±0.23	-1.85±0.17
50	-2.14±0.31	-2.53±0.27	-2.15±0.19	-1.71±0.16

REFERENCES

1. Huangfu, X.; Jiang, J.; Ma, J.; Liu, Y.; Yang, J., Aggregation Kinetics of Manganese Dioxide Colloids in Aqueous Solution: Influence of Humic Substances and Biomacromolecules. *Environ Sci Technol* **2013,** *47*, (18), 10285-10292.

2. Healy, T. W., *Colloidal silica: Fundamentals and Application*. CRC Press: Boca Raton, 2006.

3. Bahena, J. L. R.; Cabrera, A. R.; Valdivieso, A. L.; Urbina, R. H., Fluoride adsorption onto α-Al_2O_3 and its effect on the zeta potential at the alumina–aqueous electrolyte interface. *Sep Sci Technol* **2002,** *37*, (8), 1973–1987.

4. Erdemoğlu, M.; Sarıkaya, M., Effects of heavy metals and oxalate on the zeta potential of magnetite. *J Colloid Interf Sci* **2006,** *300*, 795–804.

5. Petosa, A. R.; Jaisi, D. P.; Quevedo, I. R.; Elimelech, M.; Tufenkji, N., Aggregation and deposition of engineered nanomaterials in aquatic environments: Role of physicochemical interactions. *Environ. Sci. Technol.* **2010,** *44*, (17), 6532-6549.

6. Vincent, B.; Edwards, J.; Emmett, S.; Jones, A., Depletion flocculation in dispersions of sterically-stabilised particles ("soft spheres"). *Colloids and Surfaces* **1986,** *18*, (2), 261-281.

7. Phenrat, T.; Song, J. E.; Cisneros, C. M.; Schoenfelder, D. P.; Tilton, R. D.; Lowry, G. V., Estimating attachment of nano- and submicrometer-particles coated with organic macromolecules in porous media: Development of an empirical model. *Environ Sci Technol* **2010,** *44*, (12), 4531-4538.

8. Wang, D. J.; Bradford, S. A.; Harvey, R. W.; Gao, B.; Cang, L.; Zhou, D. M., Humic Acid Facilitates the Transport of ARS-Labeled Hydroxyapatite Nanoparticles in Iron Oxyhydroxide-Coated Sand. *Environ Sci Technol* **2012,** *46*, (5), 2738-2745.

9. Lv, X.; Gao, B.; Sun, Y.; Shi, X.; Xu, H.; Wu, J., Effects of Humic Acid and Solution Chemistry on the Retention and Transport of Cerium Dioxide Nanoparticles in Saturated Porous Media. *Water, Air, & Soil Pollution* **2014,** *225*, (10), 2167.

10. Sun, B.; Zhang, Y.; Chen, W.; Wang, K.; Zhu, L., Concentration Dependent Effects of Bovine Serum Albumin on Graphene Oxide Colloidal Stability in Aquatic

Environment. *Environ Sci Technol* **2018,** *52*, (13), 7212-7219.

11. Huangfu, X.; Jiang, J.; Ma, J.; Liu, Y.; Yang, J., Aggregation kinetics of manganese dioxide colloids in aqueous solution: influence of humic substances and biomacromolecules. *Environ. Sci. Technol.* **2013,** *47*, (18), 10285-92.

12. Hong, S. K.; Elimelech, M., Chemical and physical aspects of natural organic matter (NOM) fouling of nanofiltration membranes. *J Membrane Sci* **1997,** *132*, (2), 159-181.

13. Elimelech, M.; Gregory, J.; Jia, X.; Williams, R. A., Particle Deposition and Aggregation: Measurement, Modeling, and Simulation. *Butterworth-Heinemann: Oxford, England* **1995**.

14. Israelachvili, J. N., *Intermolecular and Surface Forces*. Academic Press: London, 2011.

15. Bergstr6m, L., Hamaker constants of inorganic materials. *Advances in Colloid and Interface Science* **1997,** *70*, 125-169.

16. Faure, B.; Salazar-Alvarez, G.; Bergström, L., Hamaker Constants of Iron Oxide Nanoparticles. *Langmuir* **2011,** *27*, (14), 8659–8664.